An analysis of the growth of silver catalyzed $In_xGa_{1-x}As$ nanowires on Si (100) by metal organic chemical vapor deposition

K. Sarkar, M. Palit, S. Chattopadhyay, and P. Banerji'

Citation: Journal of Applied Physics **120**, 084309 (2016); doi: 10.1063/1.4961733
View online: http://dx.doi.org/10.1063/1.4961733
View Table of Contents: http://aip.scitation.org/toc/jap/120/8
Published by the American Institute of Physics

An analysis of the growth of silver catalyzed $In_xGa_{1-x}As$ nanowires on Si (100) by metal organic chemical vapor deposition

K. Sarkar,[1] M. Palit,[2] S. Chattopadhyay,[2] and P. Banerji[1,a)]
[1]*Materials Science Centre, Indian Institute of Technology, Kharagpur 721302, India*
[2]*Centre for Research in Nanoscience and Nanotechnology, University of Calcutta, Kolkata 700098, India*

(Received 16 June 2016; accepted 16 August 2016; published online 31 August 2016)

A model is proposed here to understand the nucleation of III–V semiconductor nanowires (NW). Whereas the classical nucleation theory is not adequately sufficient in explaining the evolution of the shape of the NWs under different chemical environment such as flow rate or partial pressure of the precursors, the effect of adsorption and desorption mediated growth, and diffusion limited growth are taken into account to explain the morphology and the crystal structure of $In_xGa_{1-x}As$ nanowires (NW) on Silicon (100) substrates grown by a metalorganic chemical vapor deposition technique. It is found that the monolayer nucleus that originates at the triple phase line covers the entire nucleus-substrate (NS) region at a specific level of supersaturation and there are cases when the monolayer covers a certain fraction of the NS interface. When the monolayer covers the total NS interface, NWs grow with perfect cylindrical morphology and whenever a fraction of the interface is covered by the nucleus, the NWs become curved as observed from high resolution transmission electron microscopy images. The supersaturation, i.e., the chemical potential is found to be governed by the concentration of precursors into the molten silver which in the present case is taken as a catalyst. Our study provides new insights into the growth of ternary NWs which will be helpful in understanding the behavior of growth of different semiconducting NWs. *Published by AIP Publishing.*
[http://dx.doi.org/10.1063/1.4961733]

INTRODUCTION

III–V compound semiconductor nanowires (NWs) have been the subject of intensive study over the past two decades due to their magnificent optical, electrical, and sensing properties. Growth of these nanowires has widely been undertaken and investigated by metal organic chemical vapor deposition (MOCVD),[1–5] molecular beam epitaxy (MBE),[6] and chemical beam epitaxy (CBE).[7,8] In all such techniques, the growth is performed either by a catalyst-assisted method or a self-catalytic method. In particle-assisted growth of III-V nanowires, a foreign metal nanoparticle is used as the promoter for the controlled 1D growth.[9–14] In a self-catalytic growth mode, the group III metal can be used as the catalyst.[15–17] Further, the growth may occur by the so called vapor-liquid-solid (VLS)[18–20] or vapor-solid-solid (VSS)[21,22] method. In VLS process, the metal catalyst is heated above the eutectic temperature and forms liquid drops of an alloy with the semiconductor substrate material. When chemical vapors are supplied, these molten catalysts collect the vapor and get supersaturated. At a specific level of supersaturation, nucleation occurs and the material is precipitated at the substrate-liquid (SL) interface. The VSS process is different from VLS only in the way that during growth the catalyst remains in a solid state and growth of NWs can occur at temperatures far below the eutectic. In both the processes, the catalyst works as a sink that adsorbs the vapor and confines the growth within its boundary on a substrate surface. The atoms can also reach the catalyst by diffusion along the NW sidewalls. In particle-assisted growth of compound NWs, radial and axial growth rate, morphology, crystallinity and composition is affected by the diffusivity, adatom mobility, and cracking efficiency of each precursor. Control over nanowire morphology and crystallinity is a prerequisite for growing nanowires that satisfy the requirements of electronic devices. Although considerable efforts have been made to study the nucleation (phenomenon) of NWs, a clear understanding on controlling the morphology and structure of NWs grown by MOCVD is still lacking.

$In_xGa_{1-x}As$ is technologically a very promising material due to its tunable direct bandgap over a wide range, high electron mobility, and tunable Schottky barrier height. It has been utilized in several kinds of applications like integrated photonic devices,[23] photovoltaics,[24] tunnel diodes,[25] photodetectors,[26,27] vertical wrap-gated field effect transistors,[28,29] tunnel field effect transistor,[30] etc. However, the growth of $In_xGa_{1-x}As$ nanowires is elusive since two group III metals with different incorporation kinetics, diffusion coefficient, and solubility are involved and a very little insight about nucleation at nano level is available. The theoretical models for NW growth which have been suggested in the literature mostly deals with the growth of Si NWs[31] and GaAs NWs[32,33] by MBE. The growth mechanism of NWs is described more conveniently in case of MBE as no precursor decomposition process is involved. Givargizov[19] proposed the first ever empirical model of VLS growth in 1973 which was later applied for explaining the growth of different semiconductor NWs. Several theoretical models for adsorption-induced VLS growth[15] and diffusion-induced VLS growth[34–37] were then evolved. Dubrovskii *et al.*, in

a)Email: pallab@matsc.iitkgp.ernet.in

their study, unified the conventional adsorption-induced model, the diffusion induced model, and nucleation-mediated growth model to explain the VLS mechanism of growth by MBE.[38] In another paper, Dubrovskii *et al*. developed a model to obtain a general expression for NW growth rate as a function of its radius and also described the transformation from cubic to hexagonal phase of NWs.[39] Glas *et al*. in their report developed a model based on the classical nucleation theory to explain the formation of wurtzite phase during the growth of NWs of semiconductors with zinc blend structure.[40] Dubrovskii and Sibirev also described the growth thermodynamics of free standing NWs in different epitaxial techniques to study the occurrence of polytypism in zinc blend III–V nanowires.[41] Plante and LaPierre in their material conservation model derived the general expressions for the time evolution of axial and radial growth.[42] All these models are capable enough to explain successfully the experimental growth of NWs, particularly the binary NWs. Few theoretical studies are available in the literature explaining the growth of III–V nanowires grown by the MOCVD technique.[43–45] However, these studies are unable to explain adequately the role of partial pressure in determining the morphology of the nanowires. In a CVD growth, the partial pressure is a function of the flow rate and the vapor pressure of the precursors. The vapor pressure, on the other hand, depends on the temperature of the bubblers which is kept constant. So to control the growth, only the flow rates can be adjusted, which in other words is the adjustment of partial pressure. Therefore, partial pressure of the precursors is a crucial parameter, the understanding of which is essential in determining the morphological evaluation of the nanowires. In this study, thus, a theoretical model is derived to understand the morphology of ternary nanowires directly from the precursor flow.

The proposed model is based on the classical nucleation theory which will be able to explain our experimental findings of growth of $In_xGa_{1-x}As$ NWs by the MOCVD technique using different TMIn/TMGa flow ratios with silver nanoparticles as catalysts. It will also analyze the effect of precursor flow rate of individual components in the chemical potential of the molten catalyst. Silver nanoparticles have been found to have an edge over gold[46] nanoparticles in growing III–V NWs as the former leads to nontapered structure and uniform composition along length.[47] In our previous report,[47] we demonstrated the growth of $In_xGa_{1-x}As$ NWs on Si (100) using silver nanoparticles as catalysts and suggested a model to explain the occurrence of single-pronged and multi-pronged NWs at two different growth temperatures. The model was based on the classical nucleation theory and could explain the role of temperature in controlling the supersaturation of the system. However, when the flow rate of the precursors is changed, essentially, due to change in chemical environment of the growth, the kinetics is disturbed and in such cases, the classical nucleation theory alone cannot explain the growth of the NWs. Thus here in this report, we have combined the adsorption induced model and the diffusion induced model with the classical nucleation theory to explain the growth of $In_xGa_{1-x}As$ NWs to account for the monolayer (ML) nucleation and dependence of its size on supersaturation.

EXPERIMENTAL DETAILS

Nanowires of $In_xGa_{1-x}As$ were grown by an atmospheric pressure MOCVD technique in a horizontal reactor using Ag nanoparticles as seeds. Nanoparticles of Ag were prepared in the form of an aqueous solution through the reduction of silver nitrate with monoethanolamine. The average size of the nanoparticles was 40 nm. The aqueous solution of nanoparticles was drop casted onto Si (100) substrates. Prior to drop casting, Si substrates were cleaned carefully employing RCA method in the following way. An aqueous solution with ammonium hydroxide and hydrogen peroxide was prepared with $NH_4OH:H_2O_2:H_2O::1:1:5$ and was heated to 70 °C. Silicon substrates were then immersed into the solution for 5 min after which the substrates were rinsed thoroughly in a de-ionized (DI) water. The native oxide layer was then etched in the buffer solution with $HF:H_2O::1:6$. The substrates were further rinsed with a plenty of DI water and dried in nitrogen ambience. After dispersing the nanoparticles on a Si surface, the substrates were transferred to a MOCVD reactor and annealed in arsine (AsH_3) atmosphere at 650 °C for 10 min to create an As rich surface. Hydrogen was used as carrier gas during growth with a flow of 4 standard liter per minute. After annealing, both the group III precursors, viz., trimethylindium (TMI) and trimethylgallium (TMG) were switched to flow to the reactor along with AsH_3. Three sets of samples were prepared with varying TMIn and TMGa flow, and they were labeled as S1, S2, and S3. The precursor flow values are in moles/min, and their partial pressures are given in Table I. The growth was performed for 5 min at 600 °C for all three sets of samples. After growth, the samples were cooled down under AsH_3 over pressure to avoid forming of As vacancies. The profile of temperature that was maintained during the growth is schematically shown in Fig. 1.

Scanning Electron Microscopy (SEM) images were obtained for each sample to examine the nature of growth and to observe the position of a catalyst in the NW structure. It was performed using a ZEISS EVO 60 Scanning Electron Microscope. Specimens for Transmission Electron Microscopy (TEM) measurements were prepared in the following manner. The NW sample was put into a glass container with ethanol. The sample in the container was kept in ultrasonic bath for 20 min in order to detach the NWs from their underlying substrate. The specimens were then dispersed onto a holey carbon film. TEM were carried out in a JEOL 3000F TEM operating at 120 kV. Bright-field TEM (BFTEM) along with selected

TABLE I. TMIn and TMGa flow conditions.

Sample code	Flow in moles/min		Partial pressure (mbar)		
	TMIn	TMGa	TMIn	TMGa	In/Ga
S1	4.46×10^{-4}	0.16×10^{-4}	2.45	88.9×10^{-3}	27.8
S2	8.92×10^{-4}	0.22×10^{-4}	4.91	123.5×10^{-3}	40.5
S3	2.0×10^{-3}	1.30×10^{-4}	11.41	741×10^{-3}	15.4

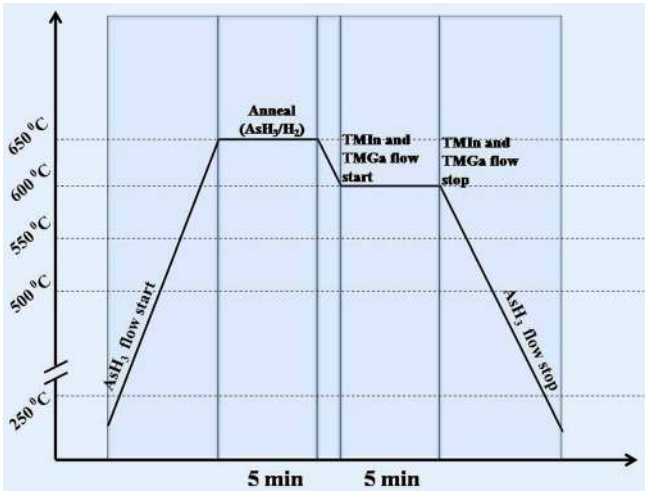

FIG. 1. Temperature-time profile of the growth process.

area electron diffraction (SAED) was employed to study the nanostructure and crystallinity of these NWs. The chemical analysis of NW ensemble was done by X-ray Photoelectron Spectroscopy using PHI 5000 VersaProbe II (ULVAC-PHI, INC, Japan) system with microfocused (100 μm, 25 W, 15 KV) monochromatic Al Kα source (hυ = 1486.6 eV), a hemispherical analyzer, and a multichannel detector. Charge calibration of binding energy scale was performed by C 1s peak at 284.6 eV.

RESULTS AND DISCUSSION

In and Ga have different solubility in silver.[48] Therefore, their concentration in the droplet catalyst is different when a constant flow of precursors through the reactor is maintained. In and Ga both are diffused through the catalyst while As reaches the nucleation site at the triple phase line (TPL) through the surface of the catalyst[49] since it does not diffuse into silver. Incorporation of group III metals also occurs through side walls of nanowires,[50] however, due to the different diffusion lengths of In and Ga,[51] they also cause unequal concentrations. Nucleation phenomenon is directly related to supersaturation which we shall attempt to correlate with the concentrations of solutes using our proposed model. A certain change in concentration alters the level of supersaturation and causes irregular nucleation into the catalyst which sometimes forbids the smooth growth of nanowires that results a perfect cylindrical morphology. The morphology of nanowires was found to change with precursor flow values, i.e., In/Ga ratio as observed from SEM images. The model is based on the classical nucleation theory that relates the morphology of the nanowires with the incorporation of two different group III materials. It is an extension of the work by Glas *et al.*[40] and Dubrovskii *et al.*[38] We have utilized nanoparticles of silver as a catalyst for nanowires growth and the solubility of precursor, i.e., their incorporation kinetics in molten silver-silicon eutectic is different. Besides, difference in adatom mobility and diffusivity on the substrate surface and NW sidewalls cause difference in incorporation, and these are assumed to be the major reasons for causing different concentration/chemical potentials into the system. In this report, we have shown that the monolayer (ML) nucleus covers the entire substrate-liquid (SL) interface at a specific level of supersaturation. When the supersaturation is higher than the critical value, the ML covers a fraction of the SL interface area. The growth of the NWs is simultaneously assisted by adsorption and diffusion, and their unequal contribution at the SL interface causes curved morphology of the NWs. We first show that the area covered by the ML at the SL interface is dependent on the chemical potential of a molten catalyst which is again a function of the concentration of elements. Next, we describe the effect of adsorption and diffusion separately in the growth of NW from vapor phase and their dependence on the flow rates of precursors. Different flow rates cause variation in the adsorption and diffusion and in turn the chemical potential which determines the ML size. Finally, we arrive at a generalized conclusion for compound NW growth that encounters the simultaneous contribution of diffusion and adsorption. Though nanowires have been found to grow below the eutectic temperature of Ag-Si system (860 °C), we have assumed the growth to be VLS since the shape of the catalysts observed by SEM is not faceted, rather spherical.[21]

Figures 2(a)–2(c) show the SEM images of nanowires grown by varying In/Ga ratio. At In/Ga ratio of 27.8, NWs are curly over few micrometers of length as shown in Fig. 2(a) while at In/Ga ratio of 40.5, NWs are found to grow with moderately curved morphology (Fig. 2(b)). At In/Ga ratio of 15.4, the growth of fine straight NWs has been observed as shown in Fig. 2(c).

The general assumptions for our proposed model are following:

(1) Adsorption of precursor into a catalyst and diffusion through a substrate and NW sidewalls separately contributes to the growth of NW.
(2) The chemical potential changes due to different concentrations of In and Ga into the liquid catalyst, since all the samples were grown at the same temperature.
(3) The growth of NWs is transport-limited.

It is a well-known fact that in VLS growth the catalyst works as a sink of precursors which dissolves the incoming vapors and at the point of supersaturation, nucleation occurs at triple phase point (TPP).[40] Under typical conditions, group III atoms diffuse from the nanowire sidewalls to the droplet but do not desorb from it, while group V species cannot diffuse along the sidewalls and easily desorb from the droplet. However, the triple phase boundary ultimately sinks the vapors.

The change in free enthalpy of the system due to nucleation of a monolayer of height h, perimeter P, and surface area A as shown in Fig. 3 is given by the equation[40]

$$\Delta G = -Ah\Delta\mu + Ph\aleph_{IL} + A(\aleph_{NL} - \aleph_{SL} + \aleph_{SN}), \quad (1)$$

where $\Delta\mu$ is the chemical potential difference of III–V pairs between liquid and solid per unit volume of the nucleus. $\aleph_{IL}$, $\aleph_{NL}$, $\aleph_{SL}$, and $\aleph_{SN}$ are the energy per unit area of the lateral surface between monolayer and liquid, nucleus-liquid, solid-liquid, and solid-nucleus interfaces, respectively.

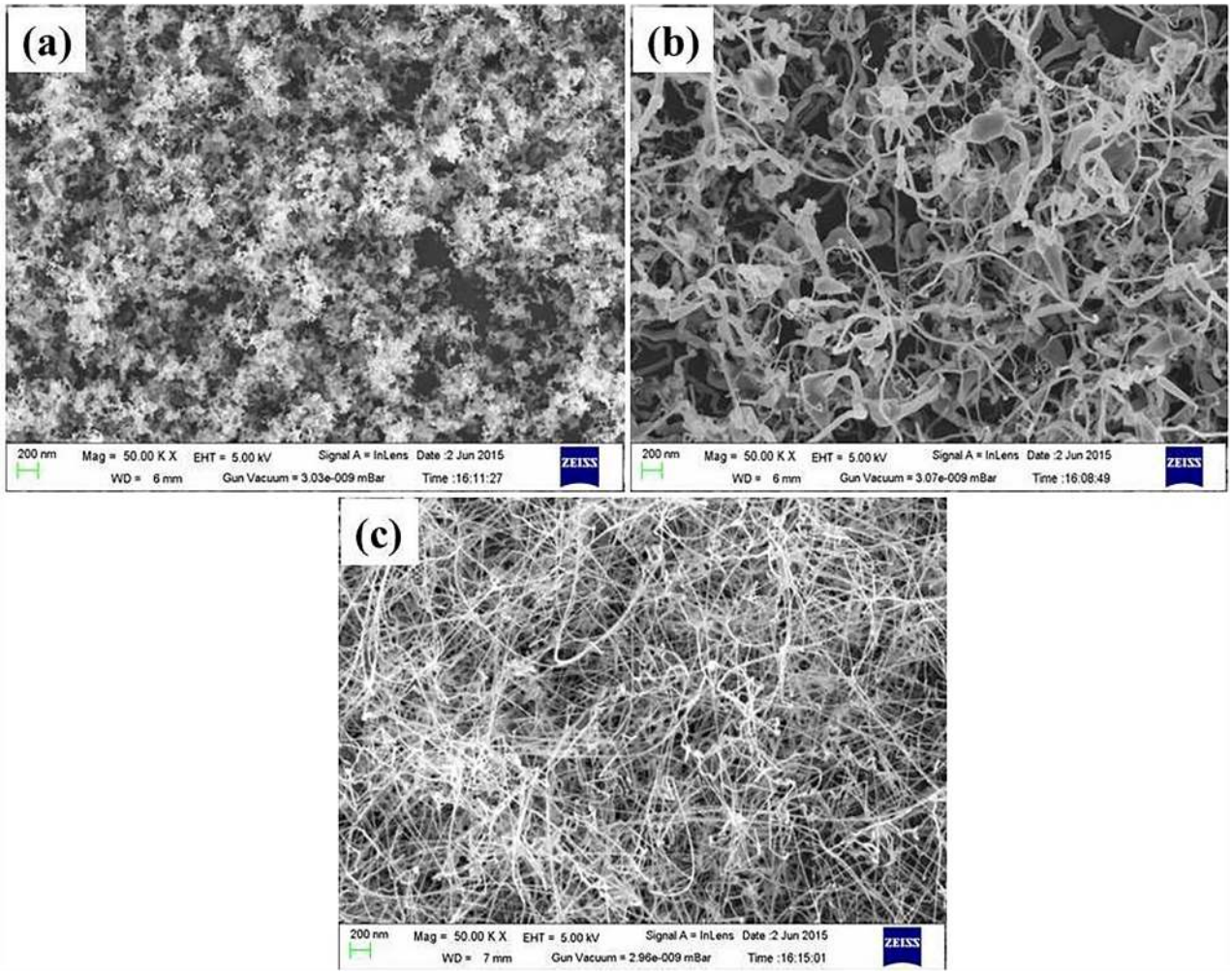

FIG. 2. FESEM images of (a) S1, (b) S2, and (c) S3.

The critical radius of the nucleus (r_N) is given by

$$r_N = \frac{h\gamma_{lL}}{\gamma_{NL} + \gamma_{SN} - \gamma_{SL} - h\Delta\mu}. \quad (2)$$

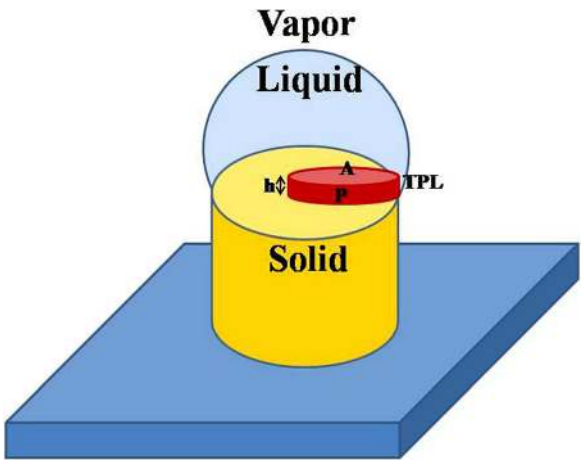

FIG. 3. Nucleation of monolayer island at triple phase boundary. The red disk is shown as the nucleus. A certain fraction of the total substrate-catalyst interface is covered at a specific level of supersaturation.

The surface energies and chemical potential decide the minimum limit of the nucleus size. In earlier reported models related to nucleation for the growth of nanowires, it has been assumed that just after the formation of nucleus at triple phase line (TPL), the nucleus rapidly spreads over the entire SL interface.[52] However, it can only happen when it is energetically favorable for the system. The nucleus, once formed, can grow either laterally or vertically, whichever promotes minimization of free energy for the system. The nucleus can either spread on the SL interface or start growing upwards, whichever is energetically favorable. This can be examined by comparing the free energies required for the nucleus to spread over with the energy required for axial growth.

We can rewrite Eq. (1) in terms of radius "r" of the nucleus as

$$\Delta G = -\pi r^2 h\Delta\mu + 2\pi r h\gamma_{lL} + \pi r^2(\gamma_{NL} - \gamma_{SL} + \gamma_{SN}). \quad (3)$$

The change in free enthalpy of the system if the nucleus grows up to radius "r'" is given by

$$\Delta G^r = -\pi h\Delta\mu(r'^2 - r^2) + 2\pi(r' - r)h\gamma_{lL} + \pi(r'^2 - r^2)(\gamma_{NL} - \gamma_{SL} + \gamma_{SN}). \quad (4)$$

Now, the change in free enthalpy of the system if the nucleus grows up to height h' is given by

$$\Delta G^h = -\pi r^2 H \Delta\mu + 2\pi r H \gamma_{lL}, \tag{5}$$

where

$$H = h' - h. \tag{6}$$

From Eqs. (4) and (5), it is concluded that the lateral growth of the nucleus costs extra energy by amount $\pi(r'^2 - r^2)(\gamma_{NL} - \gamma_{SL} + \gamma_{SN})$ which is a positive quantity. Hence, comparing Eqs. (5) and (7), we have $\Delta G^r - \Delta G^h > 0$, i.e., upward growth of nucleus is energetically more favorable compared to spreading.

Therefore, at this point, we can conclude that the nucleus does not cover the entire SL area; rather it stays at the TPL (unless the wire is very wide) and promotes growth as long as precursors are supplied. Then the question simply arises: what is the maximum radius of the monolayer? The radius of a ML is decided by the interface energies and chemical potential difference of the solid phase with the liquid phase of grown material.[48] Since chemical potential is a function of concentration, it is obvious that a certain increase or decrease in concentration (of solute) will affect the size of nucleus. Eq. (2) describes the dependence of radius of nucleus on the surface energies and chemical potential of the catalyst. The critical supersaturation can be deduced in the following manner. From the limiting condition of ML radius, we have

$$\frac{h\gamma_{lL}}{\gamma_{NL} + \gamma_{SN} - \gamma_{SL} - h\Delta\mu} \leq R, \tag{7}$$

where R is the radius of the droplet on the substrate.

The critical value of the chemical potential therefore can be expressed as

$$\Delta\mu \leq \frac{1}{h}(\gamma_{NL} + \gamma_{SN} - \gamma_{SL}) - \frac{1}{R}\gamma_{lL}. \tag{8}$$

Therefore, the supersaturation has to be greater than the critical value given in Eq. (8) to have a nucleus of radius r. Here, it is interesting to note that the ML size is dependent on the droplet size. The chemical potential required for the ML to spread over the entire substrate-liquid interface is thus derived from Eq. (8) as

$$\Delta\mu = \frac{1}{h}(\gamma_{NL} + \gamma_{SN} - \gamma_{SL}) - \frac{1}{R}\gamma_{lL}. \tag{9}$$

The conditions for ML nucleation have been derived till now by using the classical nucleation theory. However, the growth of NWs with varying morphology under different kinetics cannot be described simply by that theory. To account for the curved NW growth, we have considered the combined effect of two growth modes, viz., (i) adsorption-desorption (VLS) and (ii) diffusion through NW side walls. The growth of NWs after ML formation is thus guided by these two mechanisms simultaneously. Growth of curved NWs occurs whenever the grown material is nonuniformly distributed on the sidewalls of NW as shown schematically in Fig. 4. If at any certain portion of the nanowire sidewall, material is incorporated at rates much faster than its opposite side, then elongation in that portion would be higher due to excess material on that side compared to the opposite side. Higher accumulation of a material on the nanowire lateral surface would cause more curved structure. This phenomenon is schematically represented by two cases in Fig. 4. When the ML completely covers the nucleus-substrate (NS) interface as shown in

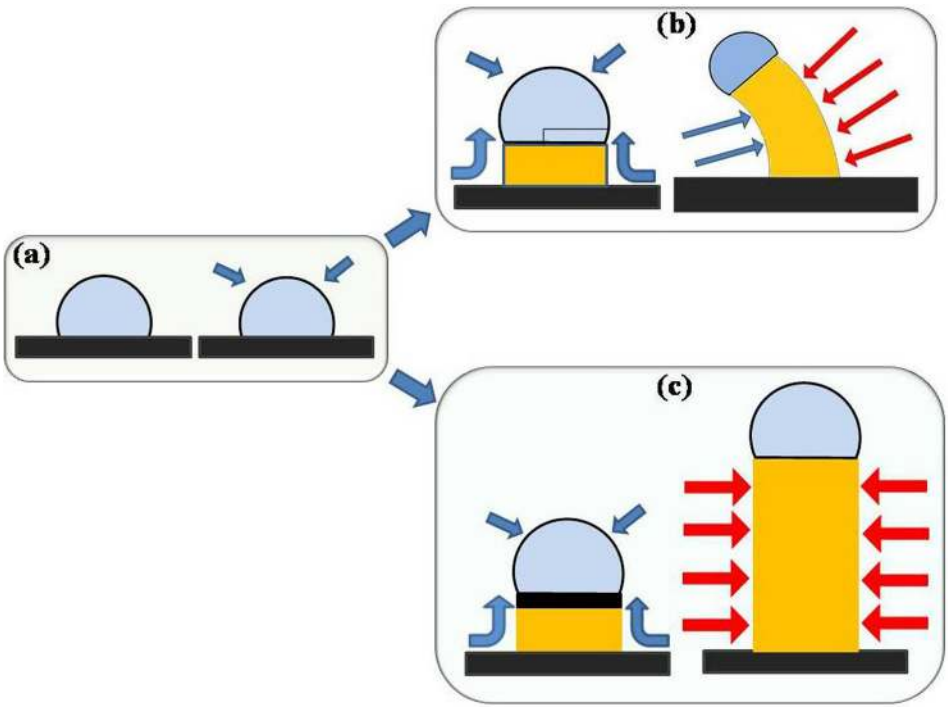

FIG. 4. Schematic of NW growth. The radius of monolayer affecting the morphology of NW. (a) The catalyst forms a droplet when heated to eutectic temperature. Supersaturation occurs after adsorbing the precursors, and nucleation occurs at TPP. (b) The nucleus covers a fraction of interface area between the catalyst and the substrate. (c) The nucleus covers the entire interface area.

Fig. 4(c), the NWs grow straight since growth occurs uniformly over the entire NS interface area. However, when the ML does not cover the NS interface completely (Fig. 4(b)), growth occurs nonuniformly at the interface. The area covered by the ML grows both by adsorption and diffusion, while on the rest of the area growth occurs only due to diffusion. Therefore, due to higher growth rate, the portion beneath the ML elongates more than the area not covered by ML, consequently giving rise to curved NWs. Now to find out the effect of ML radius on the curved morphology of $In_xGa_{1-x}As$ NWs, we estimated the contribution of each factor separately. The transport of a material in steady state adsorption mediated growth is expressed by the relation

$$\frac{\pi R^2}{\Omega_S}\frac{dL}{dt} = \pi R^2 f(\alpha,\beta)I - \frac{2\pi R^2}{1+\cos\beta}I_{des}. \tag{10}$$

The above equation was developed by Dubrovskii to describe the growth of III–V nanowires and the effect of group V element on their crystal structure through MBE.[53,54] Here, R is the radius of NW, Ω_S is the atomic volume, β is the contact angle between the droplet and the substrate surface, and $f(\alpha,\beta)$ is the amount of a material collected by a spherical droplet in a uniform flux which is a function of beam angle α and contact angle β.[51] The left hand side of this equation gives the net flux of atoms required for the elongation of NW. The first and second terms in the right hand side represent the adsorption and desorption terms, respectively, where I is the arrival rate of vapors per unit area per unit time and for MOCVD the value of the function $f(\alpha,\beta)$ is $\frac{2}{1+\cos\beta}$.[53] Now in MOCVD growth of $In_xGa_{1-x}As$, three different precursors have been used. The rate of transport of precursors through a reactor is determined by their partial pressure, molecular weight, and their incorporation into the droplet is decided by chemical activation energy and sticking coefficient. Therefore, for AsH_3, TMGa, and TMIn, the adsorption term I in Eq. (10) is represented, respectively, by the following equations as:[55]

$$J_{As_{in}} = 2\frac{P_{As_2}}{\sqrt{2\pi m_{As_2}k_BT}}S_0, \tag{11}$$

$$J_{Ga_{in}} = \frac{P_{TMGa}}{\sqrt{2\pi m_{TMGa}k_BT}}\exp\left(-\frac{E_{d,TMGa}}{k_BT}\right)S_0, \tag{12}$$

$$J_{In_{in}} = \frac{P_{TMIn}}{\sqrt{2\pi m_{TMIn}k_BT}}\exp\left(-\frac{E_{d,TMIn}}{k_BT}\right)S_0, \tag{13}$$

where P's are the partial pressure, E_d be the decomposition energy barrier of the materials, and S_0 is the sticking coefficient (=1).

Diffusion induced growth rate of NW as obtained from Dubrovski *et al.*[34,56] is expressed as

$$\frac{\pi R^2}{\Omega_S}\left(\frac{dL}{dt}\right) = -2\pi R D_f \left.\frac{dn_f}{dz}\right|, \tag{14}$$

where D_f is the diffusion coefficient and n_f is the position dependent adatom concentration on NW sidewall facets. For a particular case of vapor deposition, the net flux of materials to the top of NW for both substrate adatoms and sidewall adatoms can be calculated from the following two steady state diffusion equations:

$$D_S\Delta n_S + I\Psi_S - \frac{n_S}{\tau_S} = 0, \tag{15}$$

$$D_f\frac{d^2n_f}{dz^2} + I\Psi_f - \frac{n_f}{\tau_f} = 0, \tag{16}$$

where D_S and D_f are the adatom diffusion coefficient, respectively, on the substrate surface and sidewall facets, and τ_S, τ_f are the effective adatom lifetimes on substrate and sidewall surface, respectively. Ψ_S and Ψ_f are the temperature dependent precursor pyrolysis efficiency, respectively, on the substrate and sidewalls. The first term on the above equation defines the diffusion of adatoms, the second term represents the adsorption from the incoming vapor, and the third term gives adatom sinks.

The chemical potential in the liquid droplet with respect to solid is defined as[50]

$$\Delta\mu = \mu^l_{In} + \mu^l_{Ga} + \mu^l_{As} - \mu^s_{InGaAs}, \tag{17}$$

where μ^l_{In} and μ^l_{Ga} are the chemical potential of In and Ga atoms dissolved in the droplet, and μ^s_{InGaAs} is the solid chemical potential. These chemical potentials are in turn dependent on their relative concentrations which can be expressed by the following generalized expression:

$$\mu_x = k_BT\ln\left(\frac{P_x}{P^0_x}\right), \tag{18}$$

with P_x being the partial pressure of species "x" and P^0_x being a temperature dependent function. Although there is no concentration term in Eq. (18), however, it can surely be used for representing the concentration dependence of chemical potential since the partial pressure of a species in a gas phase is analogous to the concentration of a species in a liquid. Table I lists the values of partial pressures of TMIn and TMGa for each set of growth conditions. According to Eq. (18), the chemical potential is logarithmically related with the partial pressure (of precursor), therefore, higher the partial pressure, higher be the chemical potential. However, since we are dealing with two group III precursors, it will be convenient, for the sake of simplicity, to combine their partial pressure. Therefore, combining Eq. (18) with Eq. (17), we have

$$\Delta\mu = k_BTln\left(\frac{P_{TMIn}P_{TMGa}}{P^0_{TMIn}P^0_{TMGa}}\right) + \mu^l_{As} - \mu^s_{InGaAs}. \tag{19}$$

As we move from S1 to S3, the value of $\Delta\mu$ increases, therefore, supersaturation reduces. According to Eq. (7), the monolayer size increases with reducing supersaturation. Therefore, the nucleus covers greater area and tends to grow NWs of nearly cylindrical morphology. In case of S1 and S2, the ML radius is smaller than the radius of SL interface and therefore the grown NWs are curved. While for S3 the SL interface area is covered completely by ML and that results straight NWs. Therefore, it is observed that straight

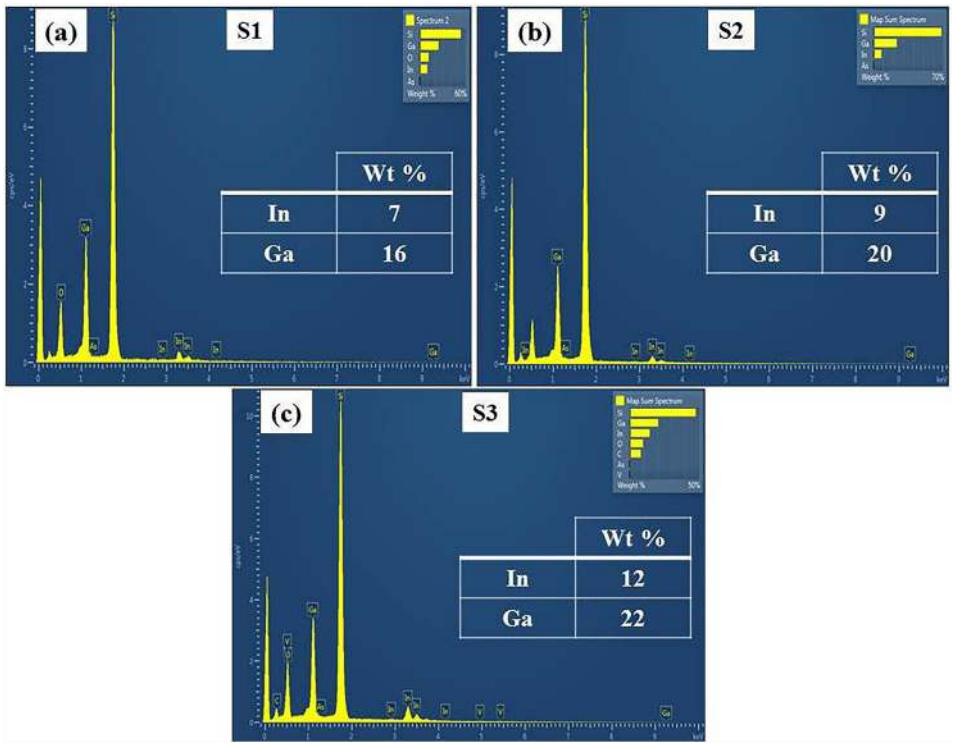

FIG. 5. EDX spectrum of (a) S1, (b) S2, and (c) S3.

cylindrical nanowires grew in sample S3 for which the partial pressure of the precursors are highest among the set of samples. For partial pressure below that level, nanowires are curved which is the case for S1 and S2. This study clearly shows that if curved nanowires are found to grow for a selected partial pressure, the morphology of the nanowires can be improved by increasing the partial pressure, i.e., flow rate of the precursors.

The energy required for thermal decomposition of TMGa and TMIn are 12 kcal/mol and 35 kcal/mol, respectively. The adsorption of TMGa is thus greater than TMIn according to Eqs. (12) and (14), when the partial pressures of both the precursors in the reactor are same. The diffusion of TMGa is again higher than that of TMIn due to smaller diffusion coefficient compared to TMGa. When the partial pressure, i.e., the flow rate is reduced, the corresponding composition of the element also reduces. It is also observed from the energy dispersive x ray (EDX) characterization that the content of both In and Ga is the highest for S3 and the lowest for S1. Figs. 5(a)–5(c) show the EDX spectra of S1, S2, and S3 respectively. According to the obtained EDX data, the content of Ga is more than that of In in all the three samples as mentioned earlier.

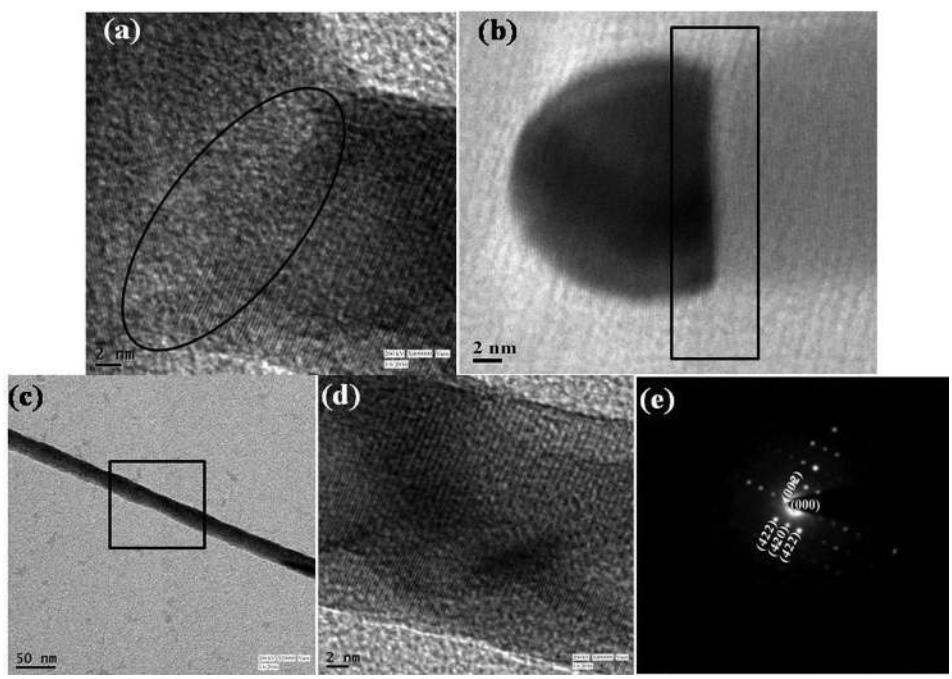

FIG. 6. (a) HRTEM image of the interface between the nanoparticle and NW for S2. It shows the case for which the nucleus covers a fraction of area on the nanoparticle-nanowire interface. (b) HRTEM image of the interface between the nanoparticle and NW for S3. It shows the case when the nucleus covers the entire interface area. (d) BF HRTEM images of S3 NW show single crystalline structure. (e) The indexed SAED pattern of S3 shows defect free zinc blend structure.

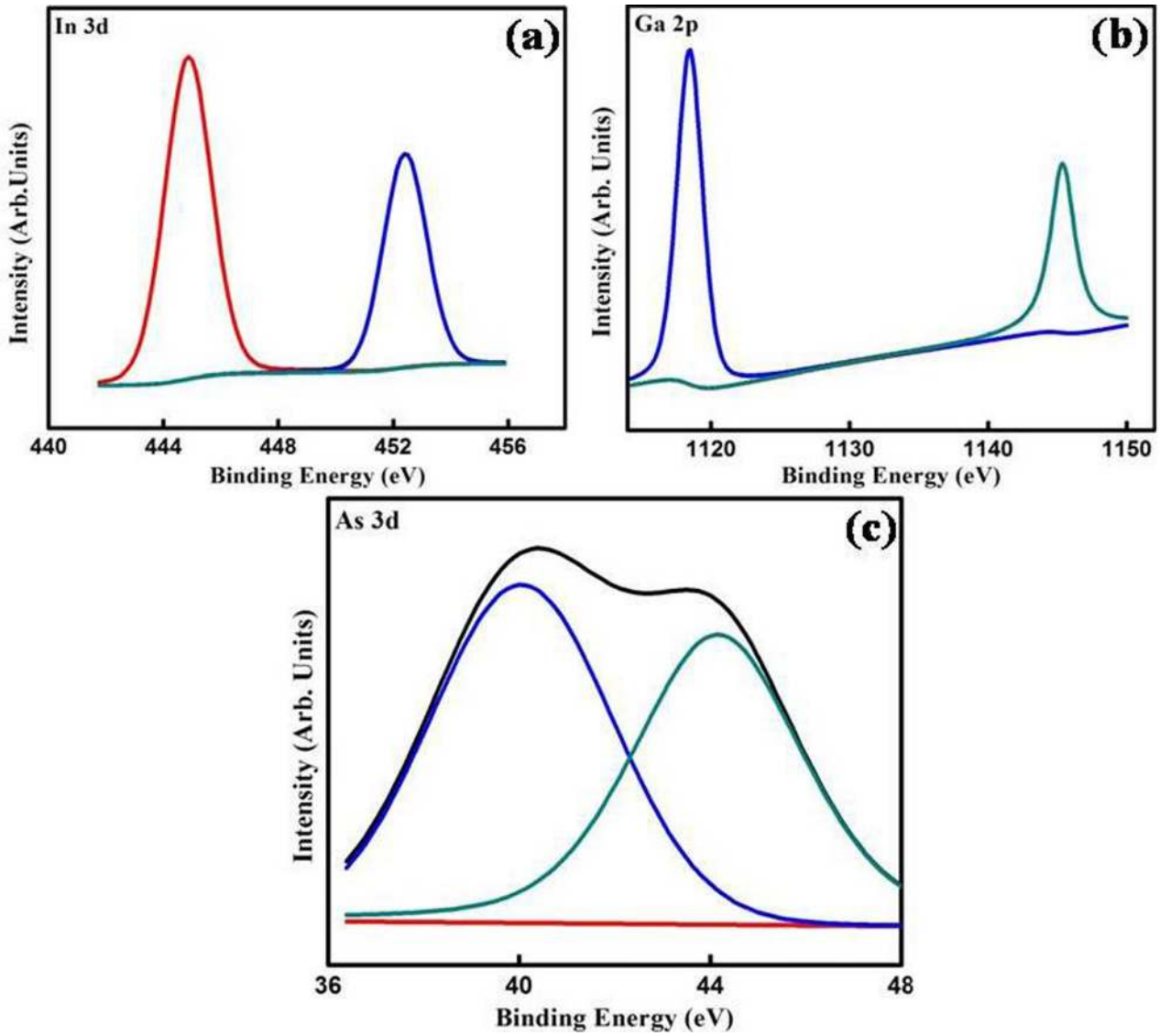

FIG. 7. XPS signals of (a) In 3d, (b) Ga 2p, and (c) As 3d.

Fig. 6(a) shows the bright field High Resolution TEM image of the interface between the catalyst and the nanowire of sample S2. Inside the encircled portion, it is observed that at the TPL the interface is not even. This here can be assumed to be the nucleus. From this image, it is evident that the ML has not covered the entire catalyst-nanowire interface area. Besides, from the HRTEM image of the catalyst-nanowire interface of sample S3, shown in Fig. 6(b), it is implied that the ML has covered the entire interface area. The TEM characterization goes well with our assumptions and ultimately validates our model giving direct evidence. Sample S3 was further characterized using TEM to study its crystalline structure since NWs with perfect cylindrical morphology are suitable for single NW device fabrication. Fig. 6(c) shows the TEM image of a NW from S3. The NW is tapering free. Fig. 6(d) shows the HRTEM image of the highlighted area. The NW is single crystalline and free from dislocations. The crystal structure is found to be zinc blend as observed from the indexed selected area electron diffraction pattern shown in Fig. 6(e).

X ray photoelectron spectroscopic analysis of S3 shows the chemical signature of the grown $In_xGa_{1-x}As$ material. As observed from Fig. 7(a), a symmetrical peak exists at 452.5 eV which is due to the $In3d^{3/2}$ state. Another symmetric peak, which is the combined characteristic peak of In bonded with GaAs and $In3d^{5/2}$, is observed at 444.9 eV. $Ga2p^{1/2}$ and $Ga2p^{3/2}$ peaks are found, respectively, at 1121.1 eV and 1148.9 eV and are shown in Fig. 7(b). Both the peaks are shifted by an amount of 4.4 eV. $As3d^{3/2}$ peak is observed at 40.0 eV in Fig. 7(c). The peak at 44.1 eV occurs due to arsenic oxide which was formed while exposing sample S3 to atmosphere.

CONCLUSION

Nanowires of $In_xGa_{1-x}As$ were grown by metal organic chemical vapor deposition with varying In/Ga ratio with silver nanoparticles on the Si substrate. Nanowires were found to grow below the eutectic temperature of a silver-silicon system. Morphology and crystallinity were found to alter with varying In/Ga ratio. This has been explained with the help of classical nucleation theory with the conventional

monolayer formation concept and combined effects of adsorption and diffusion induced growth. It has been shown that the monolayer size is a function of the chemical potential of the liquid droplet which is in turn related to the relative concentration of indium and gallium into the droplet. At a specific level of chemical potential, i.e., supersaturation, the monolayer covers the entire substrate-liquid interface and only in that situation nanowires grow in a perfect cylindrical structure since the material is incorporated uniformly over the monolayer, i.e., entire substrate-liquid area. At higher supersaturation, the monolayer size reduces and covers a fraction of the area and hence due to nonuniform incorporation of material on the substrate-liquid interface, the nanowires become curved. On the area covered by monolayer material is crystallized by both adsorption and diffusion while on the rest of the area material is incorporated only by diffusion induced process thus resulting nonuniform growth. This study thus provides optimized conditions of MOCVD grown ternary $In_xGa_{1-x}As$ nanowires, and the theory will be helpful in understanding the growth of other binary or ternary nanowires.

ACKNOWLEDGMENTS

One of the authors (K.S.) acknowledges the financial assistance from University Grants Commission (UGC). The authors acknowledge DST, New Delhi for financial support for MOCVD growth.

[1]I. Regolin, D. Sudfeld, S. Luttjohann, V. Khorenko, W. Prost, J. Kastner, G. Dumpich, C. Meier, A. Lorke, and F. J. Tegude, J. Cryst. Growth **298**, 607 (2007).
[2]J. C. Shin, D. Y. Kim, A. Lee, H. J. Kim, J. H. Kim, W. J. Choi, H. S. Kim, and K. J. Choi, J. Cryst. Growth **372**, 15 (2013).
[3]T. Sato, J. Motohisa, J. Noborisaka, S. Hara, and T. Fukui, J. Cryst. Growth **310**, 2359 (2008).
[4]Y. Kim, H. J. Joyce, Q. Gao, H. H. Tan, C. Jagadish, M. Paladugu, J. Zou, and A. A. Suvorova, Nano Lett. **6**, 599 (2006).
[5]J. Wu, B. M. Borg, D. Jacobsson, K. A. Dick, and L. E. Wernersson, J. Cryst. Growth **383**, 158 (2013).
[6]G. Koblmüller and G. Abstreiter, Phys. Status Solidi RRL **8**, 11 (2014).
[7]D. Ercolani, F. Rossi, A. Li, S. Roddaro, V. Grillo, G. Salviati, F. Beltram, and L. Sorba, Nanotechnology **20**, 505605 (2009).
[8]L. E. Jensen, M. T. Bjo, A. I. Persson, B. J. Ohlsson, and L. Samuelson, Nano Lett. **4**, 1961 (2004).
[9]T. Martensson, C. P. T. Svensson, B. A. Wacaser, M. W. Larsson, W. Seifert, K. Deppert, A. Gustafsson, L. R. Wallenberg, and L. Samuelson, Nano Lett. **4**, 1987 (2004).
[10]K. Hiruma, M. Yazawa, T. Katsuyama, K. Ogawa, K. Haraguchi, M. Koguchi, and H. Kakibayashi, J. Appl. Phys. **77**, 447 (1995).
[11]M. S. Gudiksen, L. J. Lauhon, J. Wang, D. C. Smith, and C. M. Lieber, Nature **415**, 617 (2002).
[12]J. C. Harmand, G. Patriarche, N. Pere-Laperne, M. N. Merat-Combes, L. Travers, and F. Glas, Appl. Phys. Lett. **87**, 203101 (2005).
[13]D. Gustiono, E. Wibowo, and Z. Othaman, J. Phys.: Conf. Ser. **423**, 012047 (2013).
[14]J. Wallentin, D. Kriegner, and J. Stangl, Nano Lett. **14**, 1707 (2014).
[15]Y. Jing, X. Bao, W. Wei, C. Li, O. K. Sun, D. P. R. Aplin, Y. Ding, Z. Wang, Y. Bando, and D. Wang, J. Phys. Chem. C **118**, 1696 (2014).
[16]K. A. Dick, K. Deppert, T. Martensson, B. Mandl, L. Samuelson, and W. Seifert, Nano Lett. **5**, 761 (2005).
[17]J. Tersoff, Nano Lett. **15**, 6609 (2015).
[18]E. I. Givargizov, Crystallogr. Rep. **51**, 888 (2006).
[19]E. I. Givargizov, J. Cryst. Growth **31**, 20 (1975).
[20]S. N. Mohammad, Nano Lett. **8**, 1532 (2008).
[21]C. O. Regan, S. Biswas, and J. D. Holmes, J. Mater. Chem. C **2**, 14 (2014).
[22]K. Kolasinski, Curr. Opin. Solid State Mater. Sci. **10**, 182 (2006).
[23]R. Chen, T. D. Tran, K. W. Ng, W. S. Ko, L. C. Chuang, F. G. Sedgwick, and C. Chang-Hasnain, Nat. Photonics **5**, 170 (2011).
[24]J. C. Shin, P. K. Mohseni, K. J. Yu, S. Tomasulo, K. H. Montgomery, M. L. Lee, J. A. Rogers, and X. Li, Nano Lett. **6**, 11074 (2012).
[25]T. Yang, S. Hertenberger, S. Morkoütter, G. Abstreiter, and G. Koblmuüller, Appl. Phys. Lett. **101**, 233102 (2012).
[26]L. Lin, H. L. Zhen, X. H. Zhou, N. Li, W. Lu, and F. Q. Liu, Appl. Phys. Lett. **98**, 073504 (2011).
[27]C. L. Tsai, K. Y. Cheng, S. T. Chou, and S. Y. Lin, Appl. Phys. Lett. **91**, 181105 (2007).
[28]K. Tomioka, M. Yoshimura, and T. Fukui, Nature **488**, 189 (2012).
[29]C. Thelander, L. E. Fröberg, C. Rehnstedt, L. Samuelson, and L. Wernersson, IEEE Electron Device Lett. **29**, 206 (2008).
[30]K. Tomioka and T. Fukui, Appl. Phys. Lett. **104**, 073507 (2014).
[31]L. Schubert, P. Werner, N. D. Zakharov, G. Gerth, F. M. Kolb, L. Long, U. Gosele, and T. Y. Tan, Appl. Phys. Lett. **84**, 4968 (2004).
[32]V. Dubrovskii, G. Cirlin, I. Soshnikov, A. Tonkikh, N. Sibirev, Y. Samsonenko, and V. Ustinov, Phys. Rev. B **71**, 205325 (2005).
[33]V. G. Dubrovskii, I. P. Soshnikov, G. E. Cirlin, A. A. Tonkikh, Y. B. Samsonenko, N. V. Sibirev, and V. M. Ustinov, Phys. Status Solidi B **241**, R30 (2004).
[34]V. G. Dubrovskii, N. V. Sibirev, G. E. Cirlin, I. P. Soshnikov, W. H. Chen, R. Larde, E. Cadel, P. Pareige, T. Xu, B. Grandidier, J.-P. Nys, D. Stievenard, M. Moewe, L. C. Chuang, and C. Chang-Hasnain, Phys. Rev. B **79**, 205316 (2009).
[35]V. G. Dubrovskiĭ, N. V. Sibirev, R. A. Suris, G. E. Cirlin, V. M. Ustinov, M. Tchernysheva, and J. C. Harmand, Semiconductors **40**, 1075 (2006).
[36]V. G. Dubrovskii, N. V. Sibirev, R. A. Suris, G. E. Cirlin, J. C. Harmand, and V. M. Ustinov, Surf. Sci. **601**, 4395 (2007).
[37]V. G. Dubrovskii and Y. Y. Hervieu, J. Cryst. Growth **401**, 431 (2014).
[38]V. Dubrovskii, N. Sibirev, G. Cirlin, J. Harmand, and V. Ustinov, Phys. Rev. E **73**, 021603 (2006).
[39]V. G. Dubrovskii, N. V. Sibirev, J. C. Harmand, and F. Glas, Phys. Rev. B **78**, 235301 (2008).
[40]F. Glas, J. C. Harmand, and G. Patriarche, Phys. Rev. Lett. **99**, 146101 (2007).
[41]V. G. Dubrovskii and N. V. Sibirev, Phys. Rev. B **77**, 035414 (2008).
[42]M. C. Plante and R. R. LaPierre, J. Appl. Phys. **105**, 114304 (2009).
[43]S. K. Lim, M. J. Tambe, M. M. Brewster, and S. Gradecak, Nano Lett. **8**, 1386 (2008).
[44]I. Miccoli, P. Prete, and N. Loverginea, CrystEngComm **17**, 5998 (2015).
[45]S. G. Ghalamestani, M. Ek, M. Ghasemi, P. Caroff, J. Johansson, and K. A. Dick, Nanoscale **6**, 1086 (2014).
[46]D. E. Perea, J. E. Allen, S. J. May, B. W. Wessels, D. N. Seidman, and L. J. Lauhon, Nano Lett. **6**, 181 (2006).
[47]K. Sarkar, M. Palit, P. Banerji, S. Chattopadhyay, N. N. Halder, P. Biswas, B. Nagabhusan, and S. Chowdhury, CrystEngComm **17**, 8519 (2015).
[48]F. Glas, J. Appl. Phys. **108**, 073506 (2010).
[49]P. Kratzer, S. Sakong, and V. Pankoke, Nano Lett. **12**, 943 (2012).
[50]V. Pankoke, S. Sakong, and P. Kratzer, Phys. Rev. B **86**, 085425 (2012).
[51]G. B. Stringfellow, Mater. Sci. Eng. B **87**, 97 (2001).
[52]V. Dubrovskii and N. Sibirev, Phys. Rev. E **70**, 031604 (2004).
[53]V. G. Dubrovskii, Appl. Phys. Lett. **104**, 053110 (2014).
[54]F. Glas, Phys. Status Solidi B **247**, 254 (2010).
[55]E. De Jong, R. R. LaPierre, and J. Z. Wen, Nanotechnology **21**, 045602 (2010).
[56]V. G. Dubrovskii, N. V. Sibirev, G. E. Cirlin, A. D. Bouravleuv, Y. B. Samsonenko, D. L. Dheeraj, H. L. Zhou, C. Sartel, J. C. Harmand, G. Patriarche, and F. Glas, Phys. Rev. B **80**, 205305 (2009).